Neutron removal and cluster breakup of ^{14}B and ^{14}Be

N. I. Ashwood,[1] M. Freer,[1] J. C. Angélique,[2] V. Bouchat,[3] W. N. Catford,[4,2] N. M. Clarke,[1] N. Curtis,[1] O. Dorvaux,[5] F. Hanappe,[3] Y. Kerckx,[3] M. Labiche,[6] J. L. Lecouey,[2,*] F. M. Marqués,[2] T. Materna,[3] A. Ninane,[7] G. Normand,[2] N. A. Orr,[2] S. Pain,[4] N. Soić,[1,†] L. Stuttgé,[5] C. Timis,[2,‡] A. Unshakova,[8] and V. A. Ziman[1]

[1]*School of Physics and Astronomy, University of Birmingham, Edgbaston, Birmingham, B15 2TT, United Kingdom*
[2]*Laboratoire de Physique Corpusculaire, ISMRA and Université de Caen, IN2P3-CNRS, 14050 Caen Cedex, France*
[3]*Université Libre de Bruxelles, Code Postal 226, B-1050 Bruxelles, Belgium*
[4]*School of Electronics and Physical Sciences, University of Surrey, Guildford, Surrey, GU2 7XH, United Kingdom*
[5]*Institut de Recherches Subatomique, IN2P3-CNRS/Université Louis Pasteur, Boite Postale 28, 67037 Strasbourg Cedex, France*
[6]*Department of Electronic Engineering and Physics, University of Paisley, Paisley, PA1 2BE, United Kingdom*
[7]*Institut de Physique, Université Catholique de Louvain, Louvain-la-Neuve, Belgium*
[8]*Joint Institute for Nuclear Research, 141980, Dubna, Moscow Region, Russia*

(Received 18 December 2004; published 31 August 2004)

Measurements of the neutron removal and cluster breakup cross sections for the neutron-rich nuclei ^{14}Be and ^{14}B have been performed at 34.4 and 40.8 MeV/nucleon, respectively. Enhancement of the first chance cluster breakup cross section for ^{14}Be compared to that of ^{14}B provides evidence for a well-developed He cluster structure of the ground state of ^{14}Be. Measurements of both the cross sections and decay-particle velocities suggest that multistep processes play an important role in the excitation and decay of both ^{14}B and ^{14}Be.

DOI: 10.1103/PhysRevC.70.024608 PACS number(s): 25.60.Gc, 21.60.Gx, 25.70.Mn, 27.20.+n

I. INTRODUCTION

In general, the structure of neutron-rich nuclei at the extremes of stability has yet to be fully determined. It is already clear from studies of nuclei such as ^{6}He, ^{11}Li, and ^{11}Be that there is some decoupling of the valence neutrons from a more stable core, in the form of a neutron halo. The extended spatial distribution of the valence neutrons is a property of nuclei with weakly bound neutrons in low angular momentum orbits. This decoupling may, in fact, be a general property of weakly bound neutron-dripline nuclei. For example, Horiuchi [1] has suggested that the natural state of nuclei at the dripline may be thought of in terms of islands of nuclear matter, with approximately equal numbers of protons and neutrons, embedded in a "sea" of neutrons. This clusterization of the core arises in response to the requirement for enhanced stability which necessitates that the neutron-proton overlap be maximized. Indeed, calculations have been performed of the structure of the odd mass boron isotopes $^{11-19}$B [2] using the antisymmeterized molecular dynamics (AMD) framework. This model, which allows the locations of the individual protons and neutrons to be traced, suggested that near $N=Z$ the boron nuclei are spherical and compact, whereas at the dripline (^{19}B) the nucleus becomes highly clustered. Moreover, the picture of cluster plus valence neutrons emerges in these calculations.

The nucleus ^{14}Be is the heaviest particle stable beryllium isotope, it is weakly bound ($S_{2n}=1.34$ MeV), and is believed to contain a large $\nu(2s_{1/2})^2$ admixture, with a smaller $\nu(1d_{5/2})^2$ contribution, giving rise to its halo properties [3]. Moreover, there is evidence for cluster structures with supposedly molecular characteristics (i.e., where the valence neutrons are exchanged between α-particle cores) in the lighter beryllium isotopes [4,5]. As such the ^{14}Be nucleus might also display the features predicted for ^{19}B—that is, enhanced clustering in the ground state.

The ^{14}B nucleus provides an interesting comparison. Measurements of the ^{13}B core momentum distributions following neutron removal indicate that, coupled with a low single neutron separation energy ($S_n=0.97$ MeV), the $2s_{1/2}$ orbits plays an important role, and the valence neutron has an extended distribution [6,7]. However, the AMD calculations for ^{13,15}B suggest that, although these nuclei are deformed they do not possess the high degree of clustering of ^{19}B, and by implication ^{14}B would be expected to possess a similar structure.

There is the difficult question of how to access the cluster component of the ground states of such nuclei when the cluster decay thresholds lie at excitation energies which are significantly above the ground state (greater than 9 MeV in the present case). However, if there is a well-developed cluster structure in the ground state then an enhanced inelastic excitation probability to states close to the cluster decay threshold would be anticipated. Recent calculations of the fragmentation reactions of ^{13}B and ^{19}B [8], again using the AMD model, indicate that the reaction cross sections may provide some sensitivity to the degree of clustering in the ground state.

In this paper we compare the neutron removal and breakup reactions of ^{14}B with ^{14}Be. Some of the cross-section measurements for ^{14}Be have already been published in Ref. [9]. These measurements indicate that the reaction processes are complex, but that there may be some sensitivity to the ground-state cluster structure in these nuclei. As

*Present address: NSCL, Michigan State University, Michigan 48824, USA.
†Present address: Rudjer Bošković Institute, Bijenička 54, HR-10000 Zagreb, Croatia.
‡Present address: School of Electronics and Physical Sciences, University of Survey, Surrey, GU2 7XH, UK.

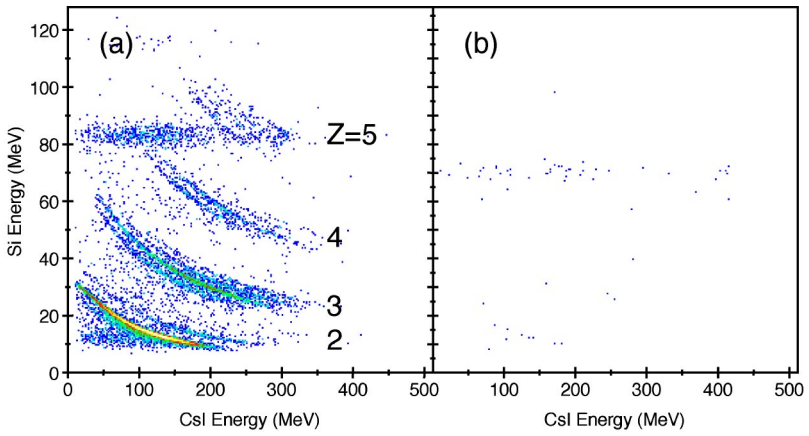

FIG. 1. (Color online) Particle identification spectra (Si energy versus CsI energy) for the ^{14}B data taken (a) with a 275 mg cm^{-2} ^{12}C target for multiplicity-2 events and (b) without a target. Note that the shift in energy is due to energy loss in the target.

such the present work should also provide a test of calculations such as those of Takemoto *et al.* [8].

II. EXPERIMENTAL DETAILS

The measurements were performed at the GANIL accelerator facility. The ^{14}Be and ^{14}B secondary beams were produced via the fragmentation of a 63 MeV/nucleon ^{18}O primary beam. The reaction products were mass, charge, and momentum analyzed using the LISE3 spectrometer resulting in beams of purities of 95% for ^{14}B and ~20% for ^{14}Be (possible contaminants to the cluster breakup channels from parasitic beams of lighter ions, most notably ^{6,8}He, were rejected in software using time-of-flight techniques) and count rates of the order of 10^4 particles per second (pps) for ^{14}B (limited by the count rate capacity of the detection system) and ~50 pps for ^{14}Be. Identification of the beam particle was achieved using time of flight through the LISE separator as measured by a parallel plate avalanche counter (PPAC) at the entrance to the reaction chamber with respect to the cyclotron rf signal. The energies of the beams were 34.4 and 40.8 MeV/nucleon for ^{14}Be and ^{14}B, respectively.

The beam was tracked onto a 275 mg cm^{-2} carbon target using two drift chambers, which provided a measurement of the position of the beam on the target with a resolution (full width at half maximum) of ~1 mm and the incident angle to within 1°. The beam and reaction products then entered a zero-degree telescope formed from two 500-μm-thick, 16-strip position-sensitive silicon detectors placed 16 cm downstream from the target. These two detectors were arranged with orthogonal strips, providing a measurement of the incident ions to $\leqslant$1 mm in both the x and y directions (the z coordinate being the beam direction). A close packed array of 16, 2.5-cm-thick, 2.5×2.5 cm^2, CsI scintillators was located behind the strip detectors. These were placed at 30 cm from the target so as to cover the same solid angle as the strip detectors as seen from the target. The telescope array spanned an angular range of 0° to 12° (to the furthest corner of the second strip detector), measured with respect to the beam axis.

Calibration of the energy response of the silicon and CsI detectors was achieved using α sources and a mixed beam of light ions of known energies. Neutrons produced in reactions of the beam were detected using an array of ~100 liquid scintillator neutron detectors (DéMoN) arranged in a similar manner to that shown in Ref. [10]. This configuration provided a single-neutron detection efficiency of ~15% (as in Ref. [3]), which is a combination of the intrinsic detection efficiency of each module and the geometric coverage folded with that of the neutron angular distributions. This efficiency was confirmed using measurements of the breakup of a ^{11}Be beam (see Ref. [9]) into ^{6}He+^{4}He+n, where the two charged fragments were detected in the zero-degree telescope. The number of neutron coincidences in DéMoN then provided a determination of the neutron detection efficiency.

Monte Carlo simulations of the response of the charged particle detection system, which included the angular distributions of the particles, indicate that the efficiency for detection of the breakup of ^{14}Be and ^{14}B into ^{x}He and ^{y}Li was 40–60 % and almost independent of the excitation energy of the decaying system over the range of excitation probed here.

III. ANALYSIS AND RESULTS

A. Charged-particle breakup processes

1. ^{14}B

The determination of the energy, mass, charge, and emission angle and thus the momenta of the charged reaction products allowed the kinematics of the reactions to be reconstructed for each event. The pixillation of the charged-particle telescope also allowed the detection of events involving multiple particles in the final state; for example, charged-particle breakup reactions. In this instance two or more fragments pass through the two silicon strip detectors. Thus, in order to correlate the particles the position information from both detectors is used and the correlated position is then mapped onto the array of CsI detectors. In this manner the energy loss, residual energy, and position may be derived for each incident fragment. Figure 1(a) shows a particle identification plot for one of the CsI detectors for the ^{14}B beam, for multiplicity-2 events. It is clear that it is possible to identify both He and Li fragments for such events using this method. Measurements with the ^{14}B beam in which the target was removed [Fig. 1(b)] demonstrate that there is negligible background in these reaction channels.

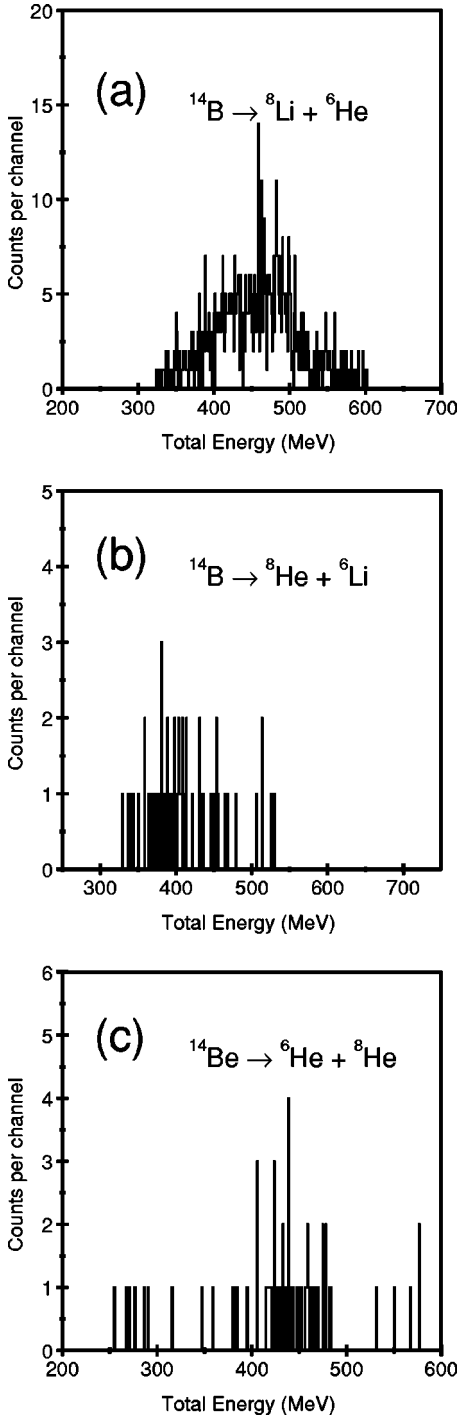

FIG. 2. Total energy spectra for the (a) $^{14}B \rightarrow {}^{8}Li + {}^{6}He$, (b) $^{14}B \rightarrow {}^{8}He + {}^{6}Li$, and (c) $^{14}Be \rightarrow {}^{6}He + {}^{8}He$ reactions.

For the breakup of ^{14}B into ^{8}Li+^{6}He or ^{6}Li+^{8}He it is possible to reconstruct the energy of the unobserved recoil particle from the measured momenta of the two detected decay products, via momentum conservation. Figure 2 shows the total energy spectra for these two decay processes reconstructed assuming a ^{12}C recoil particle. Here the total energy E_{tot} is given by $E_1+E_2+E_{\mathrm{recoil}}$, where $E_{1,2}$ are the energies of the two detected fragments, and $E_{\mathrm{tot}}=E_{\mathrm{beam}}+Q_3$, where Q_3 is the three-body reaction Q value. The resolution with which it is possible to reconstruct the total energy is limited by the knowledge of the interaction point in the target, as this determines the energy loss and straggling of the beam and reaction products. Given the 275 mg cm^{-2} target thickness, Monte Carlo simulations of the reaction and detection processes suggest a resolution of the order of 40 MeV. Thus, in the case of the inelastic scattering followed by the breakup of $^{14}B^{*}$ into ^{6}He+^{8}Li or ^{8}He+^{6}Li in which these particles were produced in their ground states and the target recoil was also left in the ground state, the yield would lie in the region $\sim$510 to $\sim$550 MeV (taking into account the energy loss in the target). In both the total energy spectra in Figs. 2(a) and 2(b) there is some yield in this energy region. However, the bulk of the yield lies between 300 and 500 MeV. Such low total energies indicate that the reactions producing the detected final states are in fact rather complex, and do not involve an intact ^{12}C recoil particle. For example, reactions such as proton transfer involving pickup of particles from the target producing an excited heavier isotope which then decays by particle emission to particle-unbound states in ^{14}B would contribute to the spectrum. Alternatively, it is possible that even more complex processes related to an intermediate compound system or target fragmentation may play a role.

In the present case, it is no longer possible to distinguish the resonant breakup of the projectile-like particle, in which the target remains bound, from higher order processes in which the target becomes excited and breaks up, or in which there is a more than three-body final state. However, the reaction products detected in the present measurements are observed at forward angles and are selected to be those with high velocities and thus it is unlikely that the coincidences arise from the dissociation of the target.

For the two-body cluster (or first chance) decay of the projectile nucleus, in which the two charged particles are detected, it is possible to reconstruct the excitation energy of the projectile prior to breakup, by measuring the invariant mass of these two fragments. This is achieved by measuring the relative energy between the breakup particles and where the excitation energy E_x is given by

$$E_x = E_{\mathrm{thresh}} + E_{\mathrm{rel}}. \tag{1}$$

Here, E_{thresh} is the threshold for the decay process (e.g., in $^{14}B \rightarrow {}^{8}Li + {}^{6}He$, $E_{\mathrm{thresh}}=14.873$ MeV) and

$$E_{\mathrm{rel}} = \frac{1}{2}\mu v_{\mathrm{rel}}^2, \tag{2}$$

where μ is the reduced mass of the system and v_{rel} is the relative velocity for the breakup particles. Equation (2) is related via the cosine rule to the mass and energy of the detected particles and the opening angle between the two fragments. This method is further described in Ref. [11] and references therein. However, in principle, it is possible to reconstruct not only the excitation energy of the projectile nucleus, but also that of a projectile-like nucleus which is populated above the cluster breakup threshold, after neutron (or proton) emission or transfer from the projectile. This is discussed in more detail in [9]. In these data it is possible that up to six undetected neutrons (less if in conjunction with

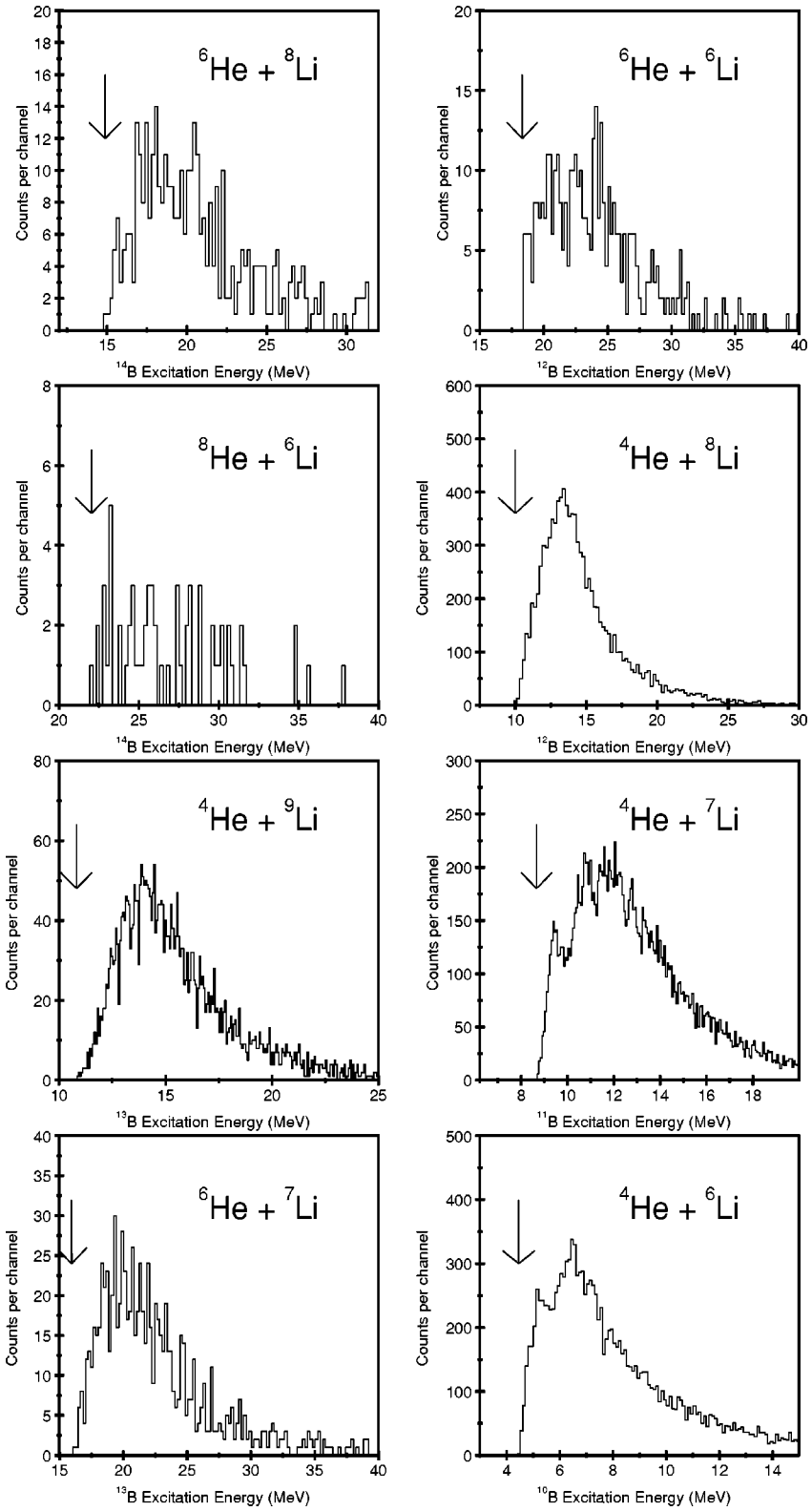

FIG. 3. Excitation energy spectra for the $^{14}B \rightarrow {}^{x}He + {}^{y}Li$ breakup channels. Arrows indicate the decay energy thresholds.

proton emission) may be emitted before the resonant nucleus undergoes He decay. Figure 3 shows the reconstructed excitation energy spectra for the ^{x}Li+^{y}He coincidences for the ^{14}B beam. The Monte Carlo simulations of the reaction and detection processes suggest that the excitation energy resolution is typically 500 keV at 1 MeV above the decay threshold and increases to ~900 keV at 3–4 MeV above threshold.

In all cases, the lower energy limits of the excitation energy spectra coincide with the decay threshold for that channel, which is an indication that the yield corresponds to the decay of the boron nucleus, rather than the coincident detec-

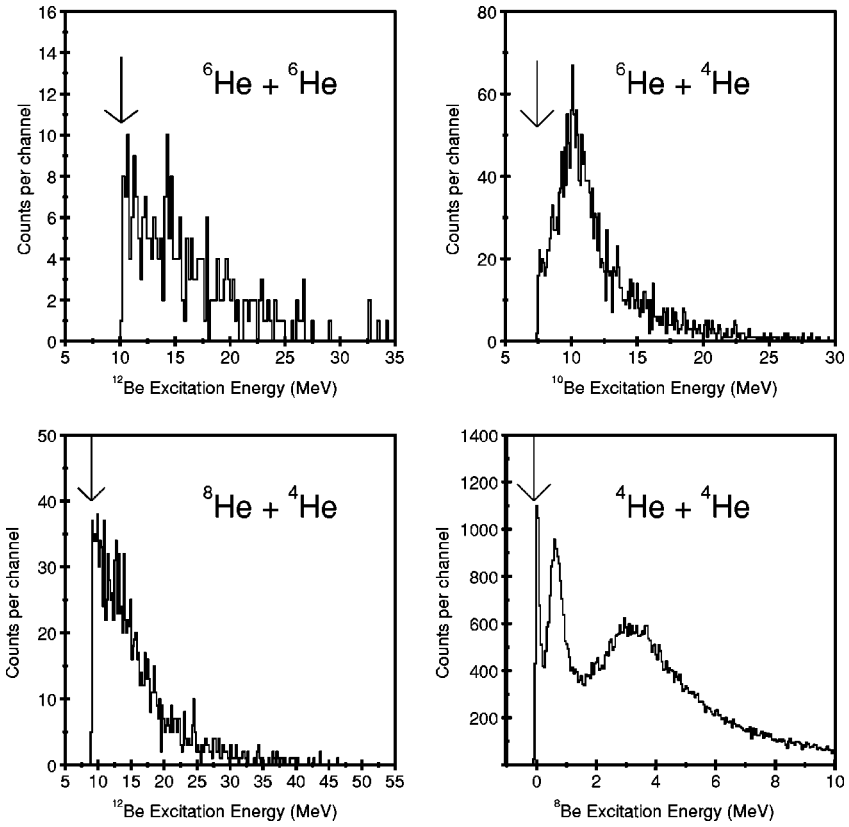

FIG. 4. Excitation energy spectra for the $^{14}B \rightarrow {}^{x}He + {}^{y}He$ breakup channels. Arrows indicate the decay energy thresholds.

tion of fragments from the projectile and the target. In most instances there is not any significant structure in the excitation energy spectra which may be linked with the decay of discrete excited states. This may be attributed to the fact that in many cases the decay process is proceeding from regions of excitation energy where there is a high density of states. In addition, the limited excitation energy resolution, which is dominated by the angular and energy straggling of the reaction products in the target and the finite position resolution of the detectors, prohibits the resolving of states with the exception of those well-separated states close to the decay threshold. The two notable exceptions are the decays of ^{10,11}B. In ^{10}B decays are observed to ^{4}He+^{6}Li from peaks at 5.1 ± 0.1 and 6.5 ± 0.1 MeV with possible evidence for a peak at 7.2 ± 0.1 MeV. These may be linked to states at 5.11 and 5.18 MeV, 6.56 MeV and 7.0 MeV, which are all known from studies of the α decay of $^{10}B^{*}$ [12]. The peaks in the ^{11}B spectrum appear at 9.4 ± 0.1, 10.7 ± 0.1, 11.9 ± 0.1, and 12.8 ± 0.1 MeV. These again coincide with known α-decaying states in this nucleus [13]. In both cases the widths of the peaks are commensurate with the predicted resolution of $\sim$500 keV close to threshold. The existence of peaks in ^{10,11}B excitation energy spectra would confirm that at least in these two cases there is a significant contribution from neutron emission processes leading to the excited states in these two nuclei prior to the α decay.

Figure 4 shows the excitation energy spectra for the coincident detection of two helium isotopes produced in reactions with the ^{14}B beam. Decays of the beryllium isotopes ^{8,10,12}Be are observed, whereas decays of the isotopes ^{9,11,13}Be cannot be reconstructed as their decay into two helium isotopes produces one fragment which is unbound against neutron decay. Once again, all of the spectra possess yield in a region of excitation energy in which helium decay processes have been previously observed. For example, ^{12}Be is known to decay into ^{6}He+^{6}He and ^{4}He+^{8}He from a series of states between 10 and 25 MeV [5,14], and ^{10}Be α decay has been found to proceed strongly from states at 9.6, 10.2, and 11.76 MeV [11,15]. In the latter case the yield is indeed concentrated around the region in which the states are known to exist, but no clear peaks are observed. This is consistent with the calculated energy resolution (800–900 keV) which is not sufficient to resolve the ^{10}Be excited states. In addition, there may be contributions from reactions which produce decay products in particle-unbound states which decay into the ^{4}He+^{6}He final state. For example, decays of ^{12}Be to $^{8}He^{*}+{}^{4}$He would proceed to a ^{4}He+^{6}He final state following the neutron decay of both $^{8}He^{*}$ and ^{7}He. In the present measurement such decay processes cannot be distinguished from those such as $p+3n$ removal followed by α decay. It is possible that direct breakup may occur which would contribute to these excitation energy spectra; however, the phase space for such processes would be relatively small.

However, the reconstructed ^{4}He+^{4}He invariant mass spectrum does show evidence for strong peaks which suggest that a large fraction of the yield is produced via the sequential decay route, i.e., the emission of protons and neutrons prior to the α decay. Two of the three peaks coincide with known states in ^{8}Be. The sharp peak at $\sim$100 keV corresponds to the decay of the ground state and the broad bump at around 3 MeV coincides with the decay of the 3.03 MeV (2^{+}) state. There exists a third peak which lies

TABLE I. Cross sections for the reactions with the ^{14}B beam. The ^{x}He+^{y}Li and ^{x}He+^{y}He channels were measured by coincident detection of the two charged fragments, while the neutron removal cross sections were measured by detecting the fragment in coincidence with a single neutron (even for events in which there was one final state neutron).

Detected particles	Cross section (b)	Threshold (MeV)
^{13}B+1n	0.193(0.013)	0.969
^{12}B+1n	0.091(0.009)	5.847
^{11}B+1n	0.060(0.007)	9.217
^{10}B+1n	$<$0.008	20.67
^{12}Be+1n	$<$0.007	16.77
^{11}Be+1n	$<$0.015	19.94
^{10}Be+1n	0.040(0.001)	20.45
^{9}Be+1n	0.013(0.001)	27.26
^{6}He+^{8}Li	$52(6)\times10^{-6}$	14.87
^{8}He+^{6}Li	$9(1)\times10^{-6}$	22.02
^{6}He+^{7}Li	$100(11)\times10^{-6}$	16.91
^{4}He+^{9}Li	$477(49)\times10^{-6}$	11.79
^{4}He+^{8}Li	$1.30(0.13)\times10^{-3}$	15.85
^{6}He+^{6}Li	$54(3)\times10^{-6}$	24.16
^{4}He+^{7}Li	$3.53(0.36)\times10^{-3}$	17.88
^{4}He+^{6}Li	$1.64(0.19)\times10^{-3}$	25.13
^{6}He+^{6}He	$38(5)\times10^{-6}$	26.88
^{8}He+^{4}He	$211(22)\times10^{-6}$	25.72
^{6}He+^{4}He	$665(68)\times10^{-6}$	27.86
^{4}He+^{4}He	$7.91(4.70)\times10^{-3}$	28.83

between the ground state and first excited state which does not correspond to a known state in ^{8}Be. This feature is consistent with the decay of the $5/2^{-}$ state in ^{9}Be to the low energy tail of the broad 2^{+} state in ^{8}Be [16,17]. The presence of this peak in the ^{8}Be decay spectrum provides a lower limit for the population of unbound states in ^{9}Be.

The cross sections for the various ^{x}Li+^{y}He and ^{x}He +^{y}He decay processes have been calculated using the detection efficiencies calculated using the Monte Carlo simulations. The calculated efficiencies are typically 40–60 % over the range of excitation energies observed in the spectra shown in Figs. 3 and 4. These relatively high detection efficiencies are a consequence of the detector telescope being placed at zero degrees and the strong kinematic focusing inherent in the high beam energy employed here. The detection efficiency does, however, fall markedly for very small relative energies as a consequence of the finite pixillation of the detection system. For example, for the decay of the ^{8}Be ground state, the small opening angle of the two α particles implies that the probability that they enter the same CsI detector is appreciable. In this instance the detection efficiency falls to 22%. The cross sections are presented in Table I, and plotted in Fig. 5. The associated decay thresholds are also given in Table I. In the case of the ^{4}He+^{4}He decay of ^{8}Be it is also possible to derive the cross sections for the decay of the ground and first excited states and also the contributions from the decay of the $5/2^{-}$ ^{9}Be state: these are 880(60), 5500(450), and 1530(120) μb, respectively. Uncertainties quoted for the cross section are statistical. The main systematic error in the determination of the cross section comes from the uncertainty in the angular distribution fall-off factor used in the Monte Carlo simulation. Calculating the efficiency at 2 MeV above the cluster decay threshold, the two-particle detection efficiency increases by ~20% for a reduction ~50% in the angular fall-off factor. Uncertainties also arise in the efficiency of the PPAC which was used to provide a measure of the number of beam particles (estimated to be ~5%). These factors result in a systematic scaling of the data and are not included in the uncertainties in Tables I and II, which are a reflection of the statistical uncertainties only.

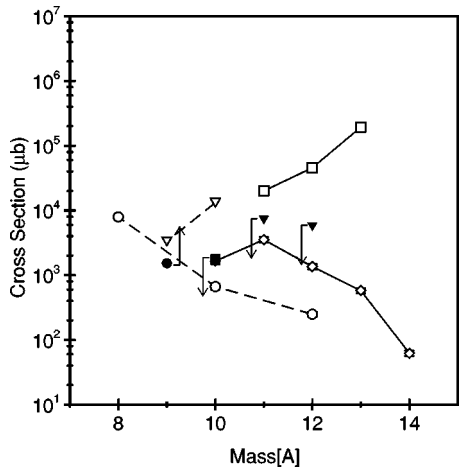

FIG. 5. ^{x}B+1n (squares), ^{x}Be+1n (triangles), ^{x}He+^{y}Li (diamonds), and ^{x}He+^{y}He (circles) cross sections for the ^{14}B beam. Closed symbols indicate cross-section limits with arrows indicating whether the cross section should lie above or below the limit. The neutron removal channels are normalized by dividing by the difference in the number of neutrons between the observed fragment and the projectile. Note that the points for the ^{9}Be breakup are lower limits deduced from the 600 keV peak in the ^{8}Be spectrum in Fig. 4.

2. ^{14}Be

It is possible to perform a similar analysis for the reactions from the ^{14}Be projectile. In this case only the coincidences between helium fragments have been reconstructed. Figure 2(c) shows the total energy spectrum for the breakup of ^{14}Be into ^{8}He+^{6}He. In this instance the total energy resolution is estimated to be ~30 MeV, and for breakup reactions in which the target recoil is left in the ground state the yield is calculated to lie between approximately 445 and 475 MeV. There is a larger fraction of the yield in this region than is observed in the corresponding ^{14}B breakup spectra. Moreover, there is a distinct difference between the ^{14}Be and ^{14}B total energy spectra, with the mean total energy lying much closer to that predicted by the Monte Carlo simulations (assuming an intact target recoil in the ground state) in the case of ^{14}Be. This is indicative of a difference in the reactions producing the final states for the two projectiles.

Figure 6 shows the reconstructed excitation energy spectra for the different possible channels. The yield in the ^{8}He

TABLE II. Cross sections for the reactions with the ^{14}Be beam. The ^{x}He+^{y}He channels were measured by coincident detection of the two charged fragments, while the neutron removal cross sections were measured by detecting the fragment in coincidence with a single neutron. Note that the neutron removal cross sections are upper limits only. The neutron removal cross sections from Refs. [3,20] are also listed for comparison.

Detected particles	Cross section (b)	Cross section (b) [3,20]	Threshold (MeV)
^{12}Be+1n	<2.33	0.75(0.01)	1.12
^{11}Be+1n	<0.69		4.29
^{10}Be+1n	<0.83	0.42(0.01)	4.79
^{8}He+^{6}He	$1.17(0.20)\times10^{-3}$		9.09
^{6}He+^{6}He	$1.33(0.22)\times10^{-3}$		11.23
^{8}He+^{4}He	$2.15(0.30)\times10^{-3}$		10.06
^{6}He+^{4}He	$10.04(0.65)\times10^{-3}$		12.20
^{4}He+^{4}He	$41.09(1.54)\times10^{-3}$		13.17

+^{6}He coincidence spectrum lies in a region of excitation energy in which states have previously been observed by Saito *et al.* [14] at 10.8, 11.6, and 15.5 MeV, although the yield in the present measurement is not sufficient to draw any further conclusions. Similarly, the yield in the ^{4}He+^{8}He and ^{6}He +^{6}He spectra for the ^{12}Be beam [5,18], and the excitation energy spectrum for ^{4}He+^{6}He coincidences overlap strongly with known breakup states in ^{10}Be [17]. The spectrum with the strongest evidence for peaks again corresponds to the decay of ^{8}Be into two α particles. As in the case of the ^{14}B projectile there is evidence for the decay of the ^{8}Be ground state and first excited state, and also the contribution from the decay of the $5/2^{-}$ ^{9}Be state to the tail of the broad 2_1^+ state in ^{8}Be. The cross sections for these reactions are given in Table II and are plotted in Fig. 7.

B. Neutron breakup channels

As noted earlier the DéMoN detector array permitted the reconstruction of neutron–charged-particle coincidences, such as the neutron removal reactions from ^{14}Be leading to the production of $^{10-13}$B fragments. Alternatively, the ^{14}B nucleus may lose both a proton and several neutrons leading to the production of beryllium isotopes $^{9-12}$Be. Figure 8(a) shows the particle identification spectrum for the ^{14}B beam incident on the carbon target, for coincidences with a neutron. In this spectrum the total energy of the particle is plotted against particle identification (PID). which has arbitrary units and the form

$$\mathrm{PID} = \left(\frac{E+\Delta E}{D}\right)^{n} + \left(\frac{E}{D}\right)^{n} \tag{3}$$

where

$$n = B - C(\Delta E/T) \tag{4}$$

and ΔE is the energy loss in the strip detectors, E is the total energy of the particle, T is the target thickness in mg cm^{-2}, $B=1.67$, $C=0.02$ (in units of mg cm^{-2} MeV), and D is a normalization parameter (in this case $D=1$ MeV). Equation (3) is an empirical power law based on the range-energy relationship of light nuclei. In this case the variables B and C were chosen so as to improve the isotopic resolution. This method is described in full in Ref. [19]. In Fig. 8(b) the same spectrum is displayed for the target out measurement. In this latter spectrum, reactions of the ^{14}B projectile in the zero-degree telescope which produce coincident neutrons appear as a distribution extending to smaller values of the total energy. Thus, in order to calculate the cross sections for reactions from the target the contributions arising from reactions in the telescope must be subtracted using the yields from the target out measurements. In the case of the Be, Li, and He isotopes the background is much less significant, and the subtraction procedure is straight forward. In order to calculate the neutron cross sections the charged-particle fragments were detected in coincidence with a single neutron and the neutron angular distributions fitted with a Lorentzian line shape, which was then integrated over the full angular range. This is the same procedure and is consistent with that performed in Ref. [9] and further described in Ref. [3]. In the case of neutron coincidences with boron fragments this analysis was performed on the background subtracted data. The resulting cross sections are shown in Table I. The cross section for the one-neutron removal agrees well with a 1n-knockout study [7], in which the cross sections to the ^{13}Be neutron-bound states were measured. In this instance the total experimental cross section was 176(16) mb. In the present data the cross section is 193(13) mb, albeit sensitive to slightly different reaction processes[1] and performed at 40.8 MeV/nucleon rather than 60 MeV/nucleon.

In the case of the ^{14}Be projectile there were no measurements of the neutron yields made without the reaction target, and thus the present measurements provide upper limits only (for the neutron removal cross sections). However, measurements of these cross sections, including the background subtraction, have already been made by Labiche *et al.* [3,20] at 35 MeV/nucleon, and these values are listed in Table II. Given an analysis of the target out yield from the ^{12}Be data taken with the present setup [9] ($\sim$20–30 % of events in the 2n-removal channel are from the target—the remainder being from reactions within the detectors), the present cross

[1]Diffractive breakup only, as opposed to absorption and diffraction [3].

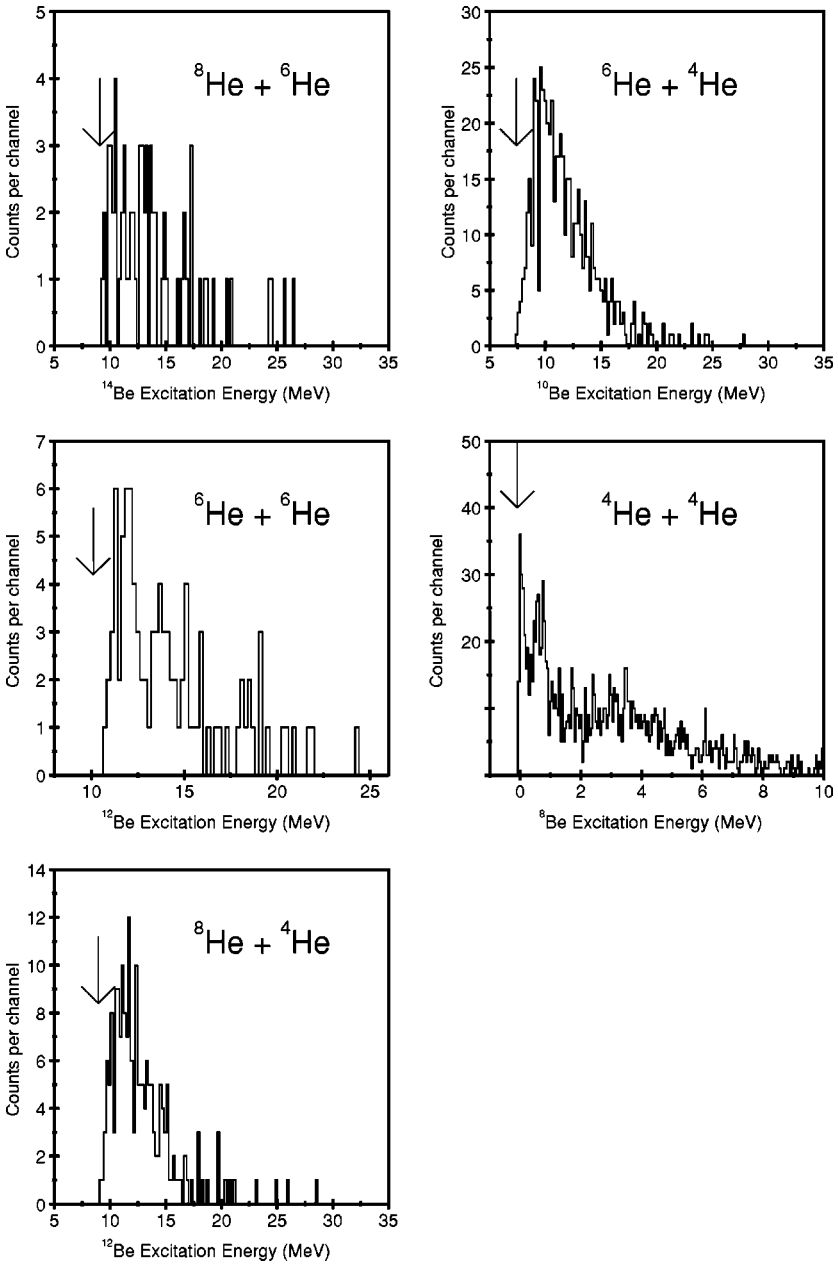

FIG. 6. Excitation energy spectra for the $^{14}\mathrm{Be}\rightarrow{}^{x}\mathrm{He}+{}^{y}\mathrm{He}$ breakup channels. Arrows indicate the decay energy thresholds.

sections are consistent with those measured by Labiche *et al.* Uncertainties quoted for the neutron breakup channels, like those for charged-particle breakup, are statistical. However, there is also an added systematic uncertainty as the neutron angular distributions vary over each decay step and thus the efficiency is not constant (there is a 17% change in the angular distribution between one-, two-, and three-neutron removal from ^{12}Be [9]).

IV. DISCUSSION

The measurement of the multineutron removal channels via the detection of the charged fragments plus one neutron presents the advantage that the detection efficiency is not prohibitively small. Naively, in this case the true cross section for the $A-Xn$ channel should be reduced by a factor X. However, the neutron angular distributions vary from decay step to decay step and thus the efficiency is not constant, and, moreover, the multiplicity of the emitted neutrons does not necessarily equal the number of missing neutrons, with the possibility of projectile neutrons interacting strongly with the target [3]. Indeed, the measured neutron multiplicities for $^{14}\mathrm{Be}\rightarrow{}^{12}\mathrm{Be}$ and $^{14}\mathrm{Be}\rightarrow{}^{10}\mathrm{Be}$ were found to be 1.63 ± 0.26 and 2.9 ± 0.8 [3,20]. Although the error bars are large these multiplicities indicate that there is a tendency for there to be somewhat fewer neutrons in the final state than anticipated. Nevertheless, for the sake of comparison with the measured helium and lithium breakup cross sections, the $^{A-X}\mathrm{B}+1n$, $^{A-X}\mathrm{Be}+1n+1p$, and $^{A-X}\mathrm{Be}+1n$ cross sections are plotted in Figs. 5 and 7 divided by X, thus indicating the strength with which the bound states of the $A-Xn$ nucleus are populated.

For the boron decay it is immediately clear, from Fig. 5, that neutron removal is favored over proton removal, and

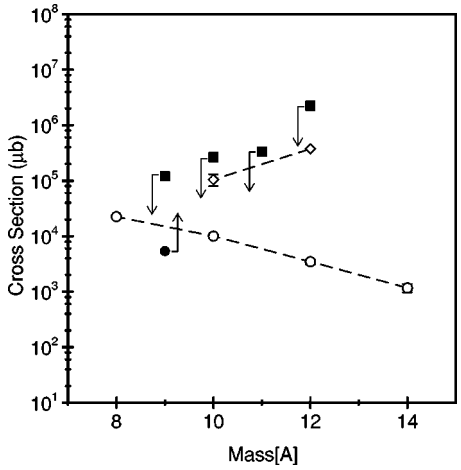

FIG. 7. ^{x}Be+1n (squares) and ^{x}He+^{y}He (circles) cross sections for the ^{14}Be beam. Closed symbols indicate cross-section limits with arrows indicating whether the cross section should lie above or below the limit. The neutron removal channels are normalized by dividing by the difference in the number of neutrons between the observed fragment and the projectile. The diamonds correspond to the measurements of Refs. [3,20].

that breakup into ^{x}He+^{y}Li is preferred over ^{x}He+^{y}He breakup. For the neutron removal reactions there is a steady decrease in the cross section as a function of the number of neutrons removed. In the case of the proton plus neutron removal cross sections these peak for the ^{10}Be+p+3n channel. The two-helium breakup yields steadily increase and peak for the $\alpha+\alpha+5n+p$ channel, which is the dominant cluster breakup mode. A similar trend is observed for the neutron removal and breakup reactions of ^{14}Be, with there being a steady decrease in the neutron removal cross sections with a corresponding growth in those for the helium breakup, again reaching a maximum for the $\alpha+\alpha+6n$ channel. It is, however, noted that only a lower limit for the decay to ^{9}Be could be found in both cases and so an increase in this cross section is expected.

There are several mechanisms by which the reaction of the boron and beryllium projectiles can proceed to the observed final states. These range from fragmentation-like processes, in which the final state products are formed in a single-step direct process proceeding via the continuum, to resonant breakup, in which excited unbound states of ^{14}Be and ^{14}B are formed which then decay into the observed final states. In addition, it is possible that there is a "cascade" effect whereby there is a buildup of certain product combinations via a sequence of decay processes proceeding via unbound states, for example, the ^{4}He+^{4}He final state may be reached by many different intermediate paths.

In order to shed some light on the possible reaction mechanisms, the measured cross sections for the breakup of both projectiles have been plotted, in Fig. 9, against the decay thresholds for the decay of the projectile into the channels listed in Tables I and II. For ^{14}B, the neutron removal cross sections (squares) appear to show an exponential trend (as indicated by the solid line) with increasing threshold, which may reflect a decreasing excitation probability for states at higher excitation. However, the remaining channels show very little correlation between the decay threshold and cross section. Indeed, the reaction channel with the highest threshold ($\alpha+\alpha+5n+p$) exhibits one of the largest cross sections. Given that even in a production mechanism by which the $\alpha+\alpha+5n+p$ final state is produced via sequential decay (i.e., the neutron decay of excited states in ^{14}B to states in ^{13}B, etc.) an excitation energy in ^{14}B of at least 28.8 MeV must be reached. This alone would make such a process highly unfavored over resonant cluster breakup such as ^{6}He+^{8}Li and ^{8}He+^{6}Li whose thresholds are 14.87 and 22.02 MeV, respectively.

For resonant, rather than sequential, breakup into an eight-body final state ($\alpha+\alpha+5n+p$) the cross section will be determined at such energies in part by phase space factors. Calculations using the Fermi breakup model [21–23] suggest that the phase space for this decay is highly constrained compared to that for direct cluster decay to, say, ^{6}He+^{8}Li and ^{8}He+^{6}Li (by 13 orders of magnitude at an excitation energy of 31 MeV). Thus it would appear that it is highly unlikely that the final state in question is arrived at via a mechanism in which the ^{14}B is resonantly excited and then decays.

Alternatively, if a transfer mechanism is invoked in which a neutron is transferred from the projectile to the target to leave an excited ^{13}B core, or two neutrons removed to leave ^{12}B, then the excitations that must be reached in these two nuclei in order to permit the decay to ^{8}Be are ~28 and ~23 MeV, respectively. These high excitations coupled with the intrinsically small transfer cross sections and the fact that

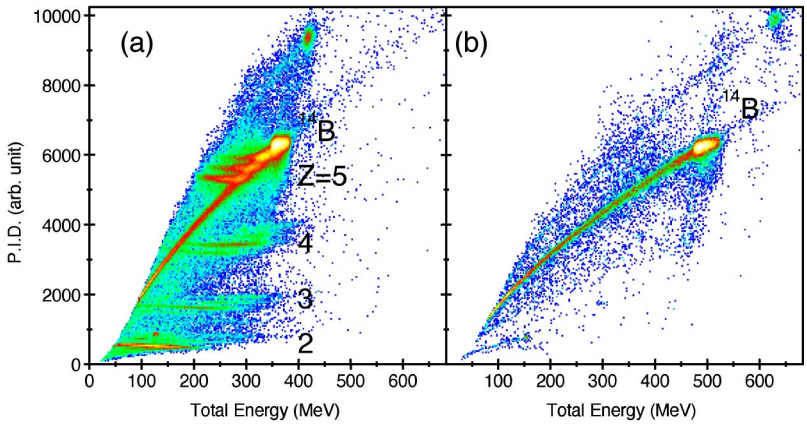

FIG. 8. (Color online) Particle identification spectra for the ^{14}B data taken (a) with a 275 mg cm^{-2} ^{12}C target and (b) without a target. Note that the shift in total energy is due to energy loss in the target.

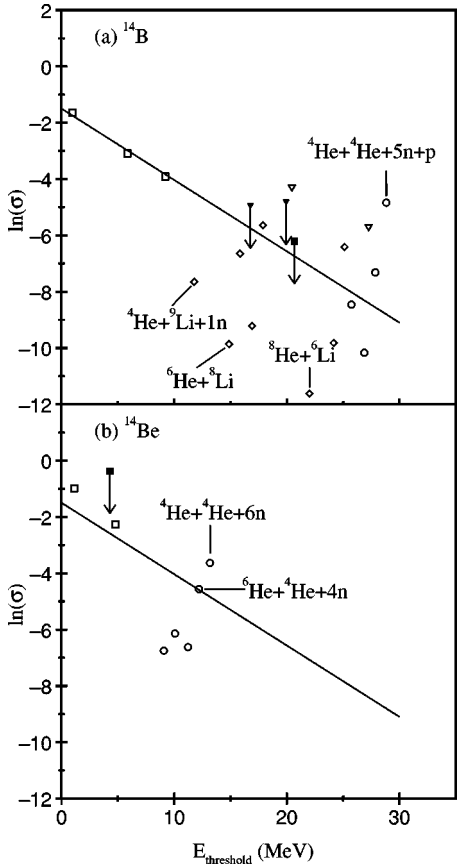

FIG. 9. Plot of $\ln(\sigma)$ versus the decay-energy threshold in the projectile nucleus for the (a) ^{14}B and (b) ^{14}Be data. In (a) the squares show the neutron removal cross sections and the triangles the $1p+Xn$ removal cross sections. The breakup into ^{x}Li+^{y}He is indicated by diamonds, and circles represent the ^{x}He+^{y}He breakup. The line indicates the trend in the neutron removal data. In (b) the neutron removal is shown by squares and the ^{x}He+^{y}He breakup by circles. The line is the trend transposed from (a). Closed symbols indicate cross-section limits with arrows indicating whether the cross section should lie above or below the limits.

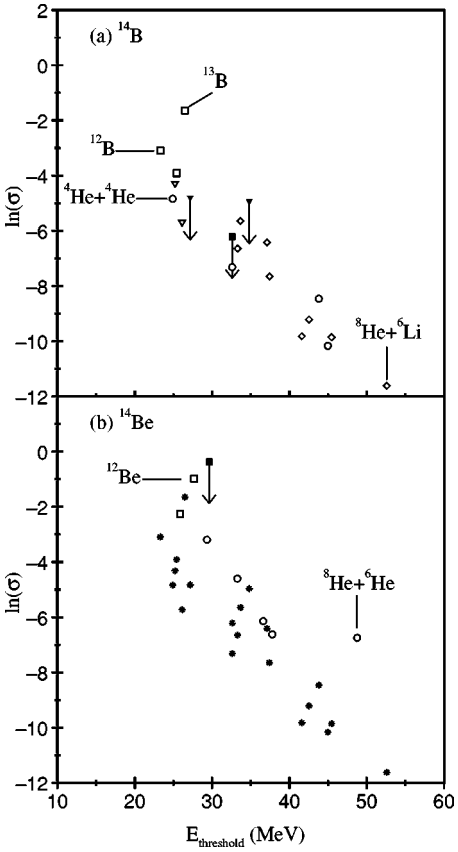

FIG. 10. Plot of $\ln(\sigma)$ versus the decay-energy threshold in the compound nucleus for (a) ^{14}B and (b) ^{14}Be. The squares show the neutron removal cross sections and the triangles the $1p+Xn$ removal cross sections. The breakup into ^{x}Li+^{y}He is indicated by diamonds, and circles represent the ^{x}He+^{y}He breakup. In (b) the neutron removal is shown by squares and the ^{x}He+^{y}He breakup by circles. Closed symbols indicate cross-section limits with arrows indicating whether the cross section should lie above or below the limits. The stars are the data points for all reactions from the ^{14}B beam, transposed from (a).

the subsequent decay process would not feed solely ^{8}Be would thus require the suppression of other reactions with more favorable decay thresholds (e.g., ^{4}He+^{8}Li decay of ^{12}B which has a threshold of 10 MeV). This would then appear to be an unlikely excitation and decay mechanism.

There remains no conventional direct mechanism by which these results may be explained. It is possible, however, that higher order intermediate processes may play a role. Certainly the total energy spectra in Fig. 2 suggest that such processes may occur. In order to investigate the possible contributions to the present reactions we have plotted in Fig. 10(a) the breakup cross sections versus the threshold in the ^{14}B+^{12}C system for the production of the $A>1$ nuclei, i.e., the breakup threshold for decay from the ^{26}Na compound nucleus into the decay channels listed in Table I (e.g., ^{26}Na$\rightarrow{}^{8}$Li+^{6}He+^{12}C, $E_{\text{thresh}}=45.441$ MeV, or ^{26}Na$\rightarrow{}^{13}$B+^{13}C, $E_{\text{thresh}}=26.591$ MeV). In all cases the thresholds have been calculated assuming that all possible excess neutrons are carried off by the undetected breakup particle rather than emitted (for the ^{4}He+^{4}He channel the number of emitted neutrons could be between 0 and 5). Despite this simplifying approximation, there now appears to be a remarkable correlation between the natural logarithms of the measured cross sections and the emission thresholds. This would also explain why there is not a large contribution to the $\alpha+\alpha$ relative energy spectrum from "feed-down" decay processes, i.e., ones in which the two α particles do not arise from the decay of ^{8}Be. There appears to be one notable exception, for the ^{14}B beam, which is the production of ^{13}B, which has a cross section that lies in excess of this trend, indicating, as one would expect, that there is a substantial component from a direct process in this case. Given the strong correlation between the cross sections and the composite (compound) system decay thresholds, there is naturally a similar correlation between the cross sections and the reaction Q-values ($Q_{\text{reaction}}=-(E_{\text{thresh}}+30.51)$ MeV for ^{14}B). Thus it is equally possible that transfer-like processes play an important role in the reaction processes. Indeed, studies of reactions producing intermediate mass fragments (IMF's) resulting from fusion-like reactions, which at intermediate energies do not proceed

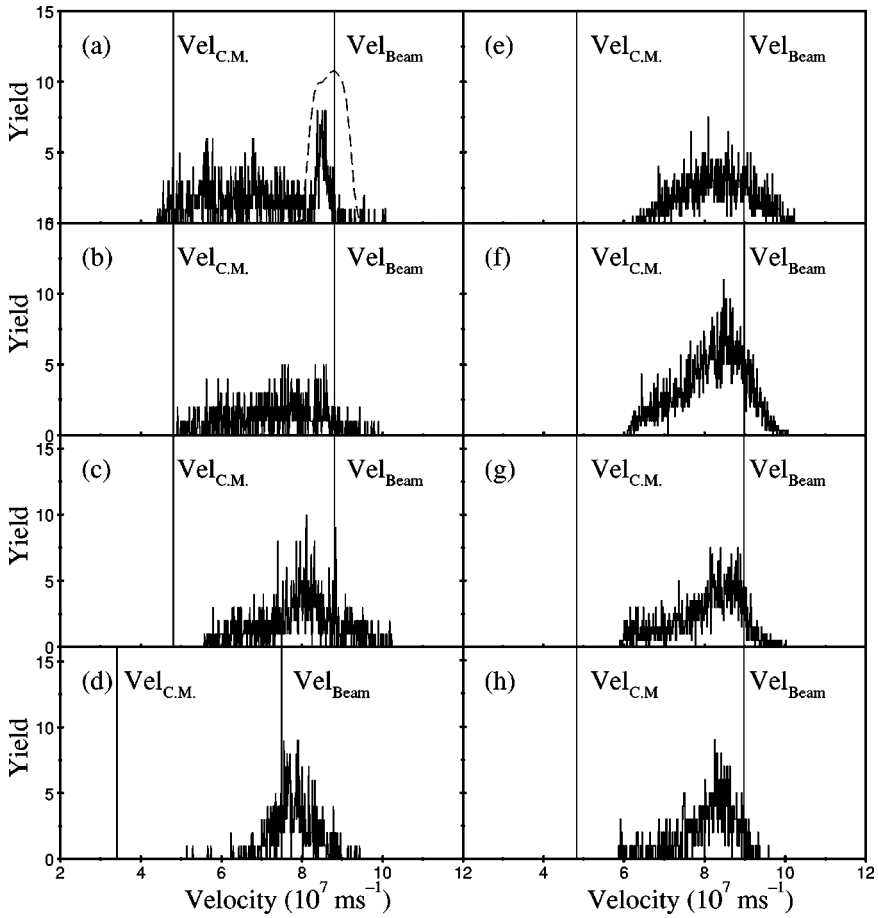

FIG. 11. Velocity distributions for (a) ^{4}He, (b) ^{6}He, and (c) ^{8}He fragments from the breakup of ^{14}B in coincidence with ^{8}He, ^{6}He, and ^{4}He, respectively. Spectrum (d) is ^{4}He from the breakup of ^{10}Be [17] detected in coincidence with ^{6}He. Velocity distributions for (e) ^{4}Li, (f) ^{6}Li, (g) ^{8}Li, and (h) ^{9}Li fragments from the breakup of ^{14}B are in coincidence with ^{4}He. Spectrum (a) shows the simulated velocities produced in the $^{14}B^* \rightarrow {}^{12}Be^* + n + p \rightarrow {}^8He + {}^4He + p + n$ reaction. Also indicated are the beam and center-of-mass velocities, Vel$_{Beam}$ and Vel$_{c.m.}$ respectively.

via the compound nucleus, are typically complex. In general, the processes fall into two categories, quasielastic (QE) and deep inelastic (DI) (see for example [24–28]). Deep inelastic collisions are dominant at large angles, greater than the grazing trajectory, and correspond to collisions in which significant mass and energy are exchanged. Typically, IMF's produced by such processes possess velocities one-third of that of the beam. Quasielastic processes dominate at small angles and correspond to less violent interactions and possess higher velocities (closer to that of the beam). These reactions are often described in terms of nucleon exchange models (see, for example, [29]). The velocities of the fragments in the present measurements may thus provide an insight into the nature of the reaction process.

Figures 11(a)–11(c) show the velocities of ^{4}He, ^{6}He, and ^{8}He nuclei produced in reactions of the ^{14}B projectile. These particles were detected in coincidence with ^{8}He, ^{6}He, and ^{4}He, respectively. Figure 11(d) displays the ^{4}He velocity distribution for the breakup of ^{10}Be in coincidence with ^{6}He. In the latter instance the data are from the measurements reported in Ref. [17], in which the reaction is believed to be inelastic excitation followed by resonant decay. In all of the plots the beam velocity and the velocity of the center-of-mass system are indicated. For the breakup of ^{10}Be into ^{6}He+^{4}He [Fig. 11(d)] it is clear that the yield is centered around the beam velocity, indicating that the excitation process is direct. On the other hand, the velocity distribution for the coincident helium nuclei produced in reactions of the ^{14}B beam lie between the beam velocity and that of the center of mass. Figures 11(e)–11(g) show a similar result for the lithium isotopes in coincidence with α particles. Also shown in the case of the ^{4}He fragments, in coincidence with ^{8}He nuclei, is the simulated distribution for ^{4}He nuclei produced in the inelastic excitation on ^{12}C of $^{14}B^* \rightarrow {}^{12}Be^* + n + p \rightarrow {}^8He + {}^4He + p + n$. These calculated velocities are peaked around that of the beam, as expected. In general, the velocity distributions for the ^{4}He and ^{6}He nuclei possess very broad distributions, but interestingly the ^{4}He distribution shows a sharp peak close to the beam velocity, which would indicate some contribution from a direct breakup process, possibly of the form simulated above, or $^{14}B^* \rightarrow {}^{10}Li^* + {}^4He \rightarrow {}^8He + {}^4He + p + n$. These systematics indicate that the reactions are neither direct nor compound in nature, but perhaps more closely related to damped processes where nucleons are exchanged between target and projectile, and the magnitudes of the exchange are largely determined by the Q values. Given that the velocities of the fragments are on average larger than half the beam velocity and extend up to that of the beam, the distributions are more characteristic of QE processes, than, say, those attributed to DI. Figure 12 thus displays the reaction cross sections plotted as a function of the transfer Q values for both ^{14}B and ^{14}Be.

Returning to the breakup of ^{14}Be, Fig. 9(b) shows again the natural logarithms of the cross sections plotted as a function of the decay threshold for the emission from the ^{14}Be projectile. A trend similar to that found for ^{14}B is apparent.

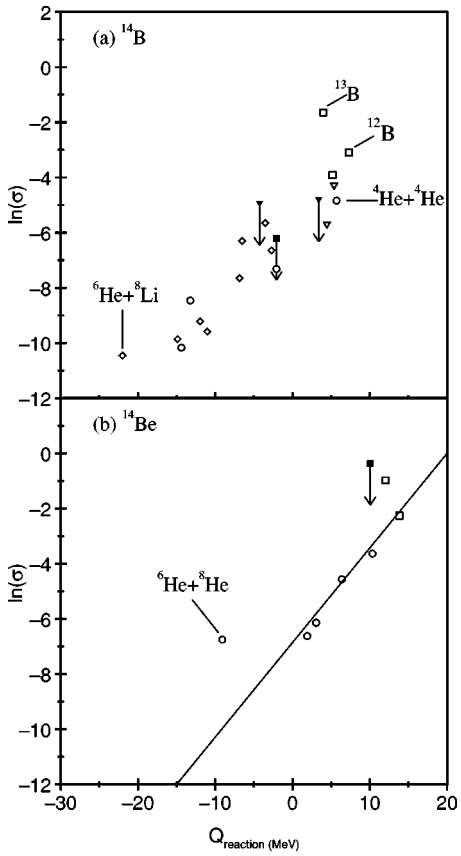

FIG. 12. Plot of $\ln(\sigma)$ versus the reaction Q values for the (a) ^{14}B and (b) ^{14}Be data. In (a) the squares show the neutron removal cross sections and the triangles the $1p+Xn$ removal cross sections. The breakup into ^{x}Li+^{y}He is indicated by diamonds, and circles represent the ^{x}He+^{y}He breakup. In (b) the neutron removal is shown by squares and the ^{x}He+^{y}He breakup by circles. Closed symbols indicate cross-section limits with arrows indicating whether the cross section should lie above or below the limits.

The neutron removal cross sections fall on a similar exponential trend (shown by the line), and the helium breakup yields show no strong correlation. On the other hand, when the yields are plotted as a function of the reaction Q value, Fig. 12(b) [or the CN decay threshold, Fig. 10(b)], the same correlation as was observed for the ^{14}B data becomes apparent. However, the $2n$-removal channel was enhanced (as expected, although the enhancement of the $3n$-removal channel is less clear as only an upper limit in the cross section could be found) with respect to this trend, as is the ^{8}He+^{6}He cluster decay channel.

This latter feature suggests that the ^{8}He+^{6}He decay of ^{14}Be is enhanced with respect to the ^{8}Li+^{6}He and ^{8}He+^{6}Li decay of ^{14}B. This in turn suggests that there is a comparatively larger direct contribution for this reaction channel, which may be a reflection of a more pronounced clusterization in the ^{14}Be ground state when compared with that occurring in ^{14}B.

V. SUMMARY AND CONCLUSIONS

Measurements of the neutron removal and cluster breakup cross sections for ^{14}Be and ^{14}B projectiles at beam energies of 34.4 and 40.8 MeV/nucleon have been performed. The coincident detection of ^{4}He, ^{6}He, and ^{8}He, from the cluster breakup of ^{14}Be, allowed the excitation energies of ^{8,10,12,14}Be to be reconstructed. Similarly, both ^{x}He+^{y}He and ^{x}He+^{y}Li coincidences were measured for reactions of the ^{14}B projectile. The reconstructed excitation energy spectra suggest that a significant fraction of the coincidence yields proceed via the decay of boron and beryllium nuclei, particularly in the case of ^{10,11}B and ^{8}Be.

The measured cross sections cannot be understood in terms of the resonant breakup of the ^{14}B and ^{14}Be beams. In fact, the cross sections for cluster breakup show no correlation with the associated decay thresholds in the two projectiles. There does, however, appear to be a correlation between the cross sections and the particle production thresholds in the composite projectile-target systems (^{26}Na and ^{26}Ne) or, alternatively, the transfer and reaction Q values. The velocity distributions of the fragments suggest that quasielastic processes play an important role in these reactions, and that the correlation should be regarded as being with the transfer and reaction Q values rather than the compound nucleus decay thresholds. This suggests that, for the majority of the reaction channels, complex multistep processes play an important role.

The one distinguishing feature between the reactions of the two projectiles is that there is an enhancement of the ^{6}He+^{8}He cluster breakup of ^{14}Be compared to that for the ^{8}Li+^{6}He and ^{8}He+^{6}Li decay of ^{14}B, in which the breakup cross sections are well described by the observed systematics. This feature may point to an enhanced breakup probability for ^{14}Be which could be related to a larger structural overlap of the ground state and states above the breakup threshold, which in turn would signal a well-developed cluster structure in the ground state.

ACKNOWLEDGMENTS

The authors are grateful to the technical and operations staff of LPC and GANIL for help in preparing and executing the experiments described here. This work was funded by the EPSRC (U. K.) and the IN2P3-CNRS (France). Additional support was provided by the Human Capital and Mobility Program of the European Community (Contract No. CHGE-CT94-0056).

[1] H. Horiuchi, in *Proceedings of the 7th International Conference on Clustering Aspects of Nuclear Structure and Dynamics* (World Scientific, Singapore, 2000), p. 405.
[2] Y. Kanada-En'yo and H. Horiuchi, Phys. Rev. C **52**, 647 (1995).
[3] M. Labiche *et al.*, Phys. Rev. Lett. **86**, 600 (2001).
[4] W. von Oertzen, Z. Phys. A **357**, 355 (1997).
[5] M. Freer *et al.*, Phys. Rev. Lett. **82**, 1383 (1999).
[6] E. Sauvan *et al.*, Phys. Lett. B **491**, 1 (2000).
[7] V. Guimarães *et al.*, Phys. Rev. C **61**, 064609 (2000).
[8] H. Takemoto, H. Horiuchi, and A. Ono, Phys. Rev. C **63**, 034615 (2001).
[9] N. I. Ashwood *et al.*, Phys. Lett. B **580**, 129 (2004).
[10] F. M. Marqués *et al.*, Phys. Rev. C **65**, 044006 (2002).
[11] N. Curtis, D. D. Caussyn, N. R. Fletcher, F. Maréchal, N. Fay, and D. Robson, Phys. Rev. C **64**, 044604 (2001).
[12] F. Ajzenberg-Selove, Nucl. Phys. **A490**, 1 (1988).
[13] F. Ajzenberg-Selove, Nucl. Phys. **A433**, 1 (1985).
[14] A. Saito *et al.*, RIKEN Accelerator Progress Report 2001, p. 55.
[15] N. Soić, S. Blagus, M. Bogovac, S. Fazinić, M. Lattuada, M. Milin, D. Miljanić, D. Rendić, C. Spitaleri, T. Tadić, and M. Zadro, Europhys. Lett. **34**, 7 (1996).
[16] Y. S. Chen, T. A. Tombrello, and R. W. Kavanagh, Nucl. Phys. **A146**, 136 (1970).
[17] S. Ahmed *et al.*, Phys. Rev. C **69**, 024303 (2004).
[18] M. Freer *et al.*, Phys. Rev. C **63**, 034301 (2001).
[19] G. W. Butler, A. M. Poskanzer, and D. A. Landis, Nucl. Instrum. Methods **89**, 189 (1970).
[20] M. Labiche, Ph.D thesis, Laboratoire de Physique Corpusculaire, LPC Report No. LPCC T 99-03,1999.
[21] E. Fermi, Prog. Theor. Phys. **5**, 1570 (1950).
[22] M. Kretschmar, Annu. Rev. Nucl. Sci. **11**, 1 (1961).
[23] M. Epherre and E. Gradsztajn, Rev. Phys. Appl. **18**, 48 (1967).
[24] M. Blann, Annu. Rev. Nucl. Sci. **25**, 123 (1975).
[25] L. Heilbronn *et al.*, Phys. Rev. C **43**, 2318 (1991).
[26] T. K. Nayak *et al.*, Phys. Rev. C **45**, 132 (1992).
[27] F. Deák *et al.*, Phys. Rev. C **39**, 733 (1989).
[28] Y. Chan, M. Murphy, R. G. Stokstad, I. Tserruya, S. Wald, and A. Budzanowski, Phys. Rev. C **27**, 447 (1982).
[29] P. J. Siemens, J. P. Bondorf, D. H.E. Gross, and F. Dickman, Phys. Lett. **36B**, 24 (1971).